Development of a model to assess acoustic treatments to reduce railway noise

H Jeong[1], G Squicciarini[1], D J Thompson[1] and J Ryue[2]

[1] Institute of Sound and Vibration Research, University of Southampton, Southampton SO17 1BJ, UK
[2] School of Naval Architect and Ocean Engineering, University of Ulsan, 93 Daehak-ro Nam-gu, Ulsan, Korea

Email: hj4g14@soton.ac.uk

Abstract. Porous materials have recently been used in absorptive treatments around railway tracks to reduce noise emissions. To investigate the effect of porous materials, a finite element model has been developed. 2D models for porous materials have been considered either as an equivalent fluid or as a poroelastic material based on the Biot theory. The two models have been validated and compared with each other to check the effect of the skeleton vibration. The poroelastic FE model has been coupled with a 2D acoustic boundary element model for use in railway applications. The results show that it may be necessary to include the frame vibration, especially at low frequencies where a frame resonance occurs. A method for the characterization of porous materials is also discussed. From this it is shown that the elastic properties of the material determine the resonance frequency and the magnitude.

1. Introduction

The dominant source of noise from railways is rolling noise, which is generated by the surface roughness of the rail and the wheel. Both the wheel and the track radiate noise through their vibration and their relative importance depends on various parameters such as the roughness spectrum, the train speed and the design of each component. Nonetheless the track component is often higher than the wheel component.

To reduce rolling noise, various measures have been developed and applied to some of the railways in operation [1]. Absorption is one of the main principles which is exploited when designing noise barriers or absorptive blocks. Porous materials are usually used in such absorptive treatments.

When analysing the performance of an absorptive treatment around the track the boundary element method is usually used as a numerical method [2, 3]. In this approach porous materials can be effectively treated as an impedance boundary. However, when they are mounted close to the rail or become parts of the railway track, it could be important to consider the elasticity of the material in the analysis, as the frame vibration could also radiate noise, rather than just absorb it. Therefore, a finite element model based on the Biot theory [4, 5] has been developed here and coupled to the acoustic boundary element method, which is used to model other components of the track.

Section 2 describes the theory and formulation of the finite element models for porous materials. Two representative models are introduced. One is the rigid frame model, which treats the porous

Content from this work may be used under the terms of the Creative Commons Attribution 3.0 licence. Any further distribution of this work must maintain attribution to the author(s) and the title of the work, journal citation and DOI.
Published under licence by IOP Publishing Ltd

medium as an equivalent fluid. In this model the frame is assumed to be rigid. The other is the elastic model, which allows the frame to move. A numerical modelling approach based on Atalla's work [6] has been implemented. This is coupled to the 2D acoustic boundary element model in Section 3 and the coupled model has been validated for both internal and external problems. Section 4 presents experimental methods for the characterisation of porous materials.

2. Finite element models for porous materials

2.1. Sound propagation in porous media having a rigid frame

When sound propagates through a porous medium, it loses energy due to viscous and thermal dissipation. In order to take this into account, parameters such as porosity, tortuosity and flow resistivity have been defined and used to characterise the dissipation mechanism. However, due to its inherent geometric complexity, it is hardly possible to describe the whole process analytically. For this reason, most of the research on porous materials has been based on phenomenological descriptions at large scale. In addition, frequency analysis is widely used. Such analysis starts from evaluating velocity and pressure in the pores, to treat the porous material as an equivalent fluid. The equivalent fluid is described by the acoustic wave equation with the density and bulk modulus replaced by a frequency-dependent effective density and bulk modulus. A range of models for effective density and bulk modulus have been proposed, and the validity of these models has also been discussed in [7]. The material is assumed to be isotropic for simplicity. The effective density and bulk modulus can be written as [7]

$$\rho = \rho_0 \left[\alpha_\infty + \frac{\nu\phi}{j\omega q_0} G(\omega)\right] \tag{1}$$

$$K = \gamma P_0 / \left[\gamma - \frac{\gamma - 1}{1 + \frac{\nu'\phi}{j\omega q_0'} G'(\omega)}\right] \tag{2}$$

where α_∞ is the static tortuosity, ν is the kinematic viscosity, ϕ is the porosity, q_0 is the static permeability, γ is the ratio of specific heats, P_0 is the ambient pressure, ν' is the thermal viscosity, and q_0' is the static thermal permeability. $G(\omega)$ and $G'(\omega)$ are frequency-dependent functions evaluated by the models. In this paper, the models of Johnson et al. [8] and Champoux-Allard [9] have been used for the density and the bulk modulus, respectively. The equations for G and G' are

$$G(\omega) = \left[1 + \left(\frac{2\alpha_\infty q_0}{\phi\Lambda}\right)^2 \frac{j\omega}{\nu}\right]^{1/2} \tag{3}$$

$$G'(\omega) = \left[1 + \left(\frac{\Lambda'}{4}\right)^2 \frac{j\omega}{\nu'}\right]^{1/2} \tag{4}$$

where Λ and Λ' are the viscous and thermal characteristic lengths. As mentioned above, the equivalent fluid has the same governing equation as the acoustic wave equation. Thus it could be used directly in the acoustic finite element formulation with the modified density and bulk modulus.

2.2. Sound propagation in porous media having an elastic frame

2.2.1. Outline of the theory. The governing equations of the sound propagation in poroelastic materials are given by the Biot theory [4, 5]. To make the problem as simple as possible, the structure of the porous material is assumed to be isotropic. Also, the deformation of the frame is supposed to be like that of an elastic solid so that the air-frame interaction can be approximated similarly to that of a rigid porous medium. Later, Atalla [6] put the equations in another form for an easier numerical implementation. These modified equations are

$$\boldsymbol{\nabla}\cdot\hat{\boldsymbol{\sigma}}^{\mathrm{s}}+\omega^2\tilde{\rho}\boldsymbol{u}+\tilde{\gamma}\boldsymbol{\nabla}p=0 \tag{5}$$

$$\boldsymbol{\nabla}^2p+\omega^2\frac{\tilde{\rho}_{22}}{R}p-\omega^2\frac{\tilde{\rho}_{22}}{\phi^2}\tilde{\gamma}\boldsymbol{\nabla}\cdot\boldsymbol{u}=0 \tag{6}$$

where $\hat{\boldsymbol{\sigma}}^{\mathrm{s}}$ is the modified stress tensor using the Biot coefficients, $\boldsymbol{u}$ is the displacement of the skeleton, p is the fluid pressure in the pores, $\tilde{\rho}$ are the effective densities, and $\tilde{\gamma}$ is related to the coupling between solid and fluid. A detailed description of the variables can be found in [7]. In each equation, the first two terms describe its motion without the effect of the other, and the third term is related to coupling between the two phases.

2.2.2. Numerical implementation. Weak integral forms are obtained by imposing an admissible displacement into Equation (5) and pressure into Equation (6), respectively. A detailed derivation is given in [6]. The results are

$$\int_V\hat{\boldsymbol{\sigma}}^{\mathrm{s}}(\boldsymbol{u}):\boldsymbol{\epsilon}^{\mathrm{s}}(\delta\boldsymbol{u})dV-\omega^2\int_V\tilde{\rho}\boldsymbol{u}\cdot\delta\boldsymbol{u}dV-\int_V\tilde{\gamma}\boldsymbol{\nabla}p\cdot\delta\boldsymbol{u}dV-\int_\Omega[\hat{\boldsymbol{\sigma}}^{\mathrm{s}}\cdot\boldsymbol{n}]\cdot\delta\boldsymbol{u}d\Omega=0 \tag{7}$$

$$\int_V\left[\frac{\phi^2}{\omega^2\tilde{\rho}_{22}}\boldsymbol{\nabla}p\cdot\boldsymbol{\nabla}\delta p-\frac{\phi^2}{R}p\delta p\right]dV-\int_V\tilde{\gamma}\boldsymbol{\nabla}\delta p\cdot\boldsymbol{u}dV+\int_\Omega\left[\tilde{\gamma}u_{\mathrm{n}}-\frac{\phi^2}{\tilde{\rho}_{22}\omega^2}\frac{\partial p}{\partial n}\right]\delta pd\Omega=0 \tag{8}$$

where $\boldsymbol{u}$ is the displacement of the solid and p is the interstitial fluid pressure in the pores. The corresponding matrices are

$$\int_V\hat{\boldsymbol{\sigma}}^{\mathrm{s}}(\boldsymbol{u}):\boldsymbol{\epsilon}^{\mathrm{s}}(\delta\boldsymbol{u})dV\rightarrow\{\delta u_i\}^{\mathrm{T}}[K]\{u_i\} \tag{9}$$

$$\int_V\tilde{\rho}\boldsymbol{u}\cdot\delta\boldsymbol{u}dV\rightarrow\{\delta u_i\}^{\mathrm{T}}[M]\{u_i\} \tag{10}$$

$$\int_V\tilde{\gamma}\boldsymbol{\nabla}p\cdot\delta\boldsymbol{u}dV\rightarrow\{\delta u_i\}^{\mathrm{T}}[\tilde{C}]\{p_i\} \tag{11}$$

$$\int_V\frac{\phi^2}{\tilde{\rho}_{22}}\boldsymbol{\nabla}p\cdot\boldsymbol{\nabla}\delta pdV\rightarrow\{\delta p\}^{\mathrm{T}}[H]\{p_i\} \tag{12}$$

$$\int_V\frac{\phi^2}{R}p\delta pdV\rightarrow\{\delta p\}^{\mathrm{T}}[Q]\{p_i\} \tag{13}$$

After substituting these into the original equations, the following coupled system is obtained:

$$\begin{bmatrix}[K]-\omega^2[M] & -[\tilde{C}]\\ -\omega^2[\tilde{C}]^{\mathrm{T}} & [H]-\omega^2[Q]\end{bmatrix}\begin{Bmatrix}u_i\\ p_i\end{Bmatrix}=\begin{Bmatrix}F_{\mathrm{s}}\\ F_{\mathrm{f}}\end{Bmatrix} \tag{14}$$

where M and K are the effective mass and stiffness matrices for the solid, H and Q are the equivalent kinematic and compression energy matrices for the fluid, $\tilde{C}$ is the coupling matrix, F_{s} and F_{f} are the loading vectors. For the poroelastic finite element, it is recommended to have more than 12 elements in one wavelength [10-12].

3. Coupling with the acoustic boundary element formulation

A standard 2D acoustic boundary element formulation has been used as presented in [13]. The matrix equation is given as

$$\begin{bmatrix}[H] & -[G]\\ [C_A] & [C_B]\end{bmatrix}\begin{Bmatrix}p\\ v_{\mathrm{n}}\end{Bmatrix}=\begin{Bmatrix}0\\ C_C\end{Bmatrix} \tag{15}$$

The first row is obtained from the Kirchhoff-Helmholtz boundary integral equation and the second row represents the boundary conditions. At the interface, continuity boundary conditions must be satisfied. This is detailed in [14]. For most porous materials, all the boundary integral terms vanish when the material is coupled to air. The only thing to be done is to impose the pressure explicitly. The resultant matrix equation becomes

$$\begin{bmatrix} [H] & -[G] & 0 & 0 \\ [C_A] & [C_B] & BC_1 & BC_2 \\ 0 & 0 & [K]_s - \omega^2[M]_s & -[\tilde{C}] \\ BC_3 & 0 & -\omega^2[\tilde{C}]^T & [H] - \omega^2[Q] \end{bmatrix} \begin{Bmatrix} p_a \\ v_n \\ u_p \\ p_p \end{Bmatrix} = \begin{Bmatrix} 0 \\ C_C \\ F_s \\ F_f \end{Bmatrix} \quad (16)$$

where BC_1 and BC_2 are the coupling terms in the boundary element formulation. Note that in the rows which represent the interface all components are zero except for those in the coupling equation.

3.1. Validation

A comparison has been made to validate the developed BE-FE code for both external and internal problems.

3.1.1. Internal problem. A calculation has been carried out for a layer of glass wool at the end of a tube as shown in Figure 1. The glass wool has been set to have a high shear modulus to behave effectively as a rigid porous material, such that the result can be compared with the analytical solution. The full properties of the sample are given in Table 1.

Table 1. Properties of glass wool [6]

Property	α_∞	ρ_s (kg/m^3)	σ (Ns/m^4)	ϕ	N (kPa)	ν	Λ (μm)	Λ' (μm)	l (cm)
Value	1.06	130	40000	0.94	2200(1+j0.1)	0	56	110	10

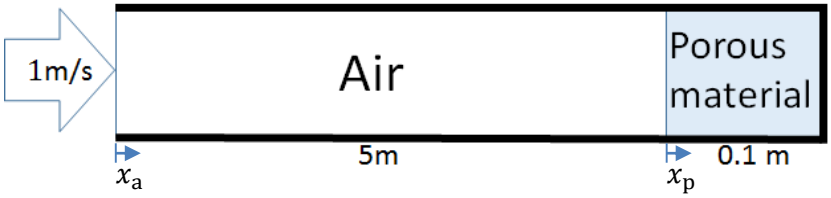

Figure 1. Rigid tube with glass wool at the end (not to scale)

For a given maximum frequency, the number of elements n_e is determined following the criteria below:

$$6 \times \Delta x_a < \lambda_{min} \rightarrow n_{ea} > \frac{6 f_{max}}{c_a} L_{xa} \quad (17)$$

$$12 \times \Delta x_p < \lambda_{min} \rightarrow n_{ep} > \frac{12 f_{max}}{c_p} L_{xp} \quad (18)$$

where the subscripts 'a' and 'p' indicate 'air' and 'porous', respectively. In this case, $f_{max} = 500$ Hz and $n_{ea} > 43.73, n_{ep} > 8.78$ with $c_a = 343\, m/s$, $\mathrm{Re}(c_p) = 68.37\, m/s$. $n_{ea} = 44$ and $n_{ep} = 10$ have been used and the results are shown in Figure 2. The analytical solution has been obtained by considering the rigid porous material as an equivalent fluid layer to validate the numerical result.

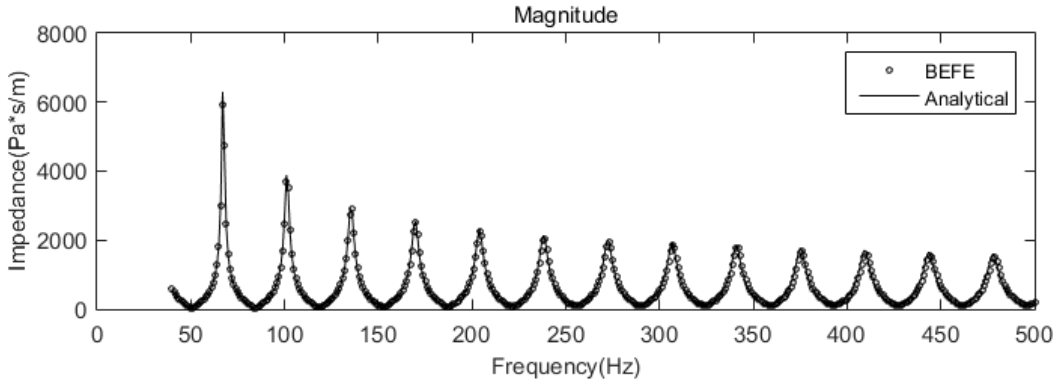

(a)

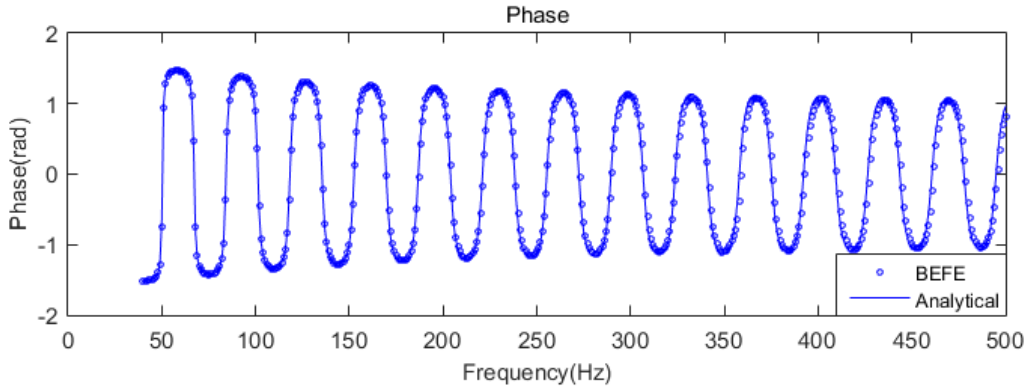

(b)

Figure 2. Input impedance with elements $(n_{\mathrm{ea}}, n_{\mathrm{ep}}) = (44,10)$: (a) Magnitude, (b) Phase

The results show the magnitude and phase of the input impedance. The lines are obtained from the analytical solution and the dots are from the numerical simulation. It can be said that the recommended criteria give acceptable agreement. From this, it can be said that the BE-FE coupled code is reliable for internal problems.

To see the effect of frame vibration, a comparison has been made between the rigid model and the elastic model in Figure 3. The two differ at around 470 Hz where the frame resonance occurs but otherwise are identical.

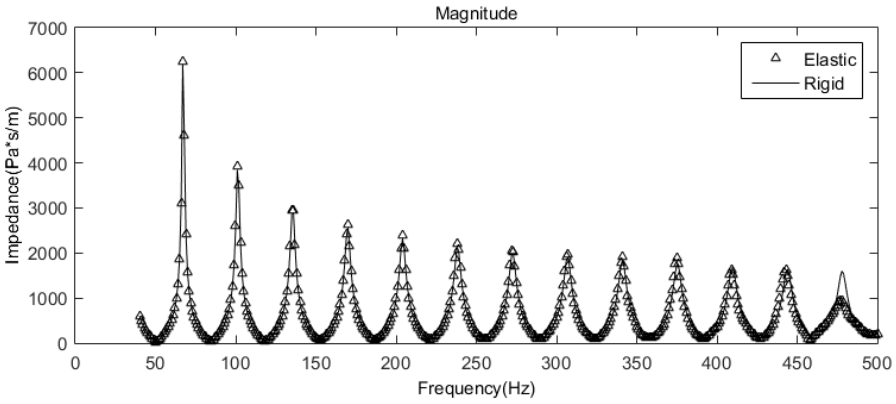

(a)

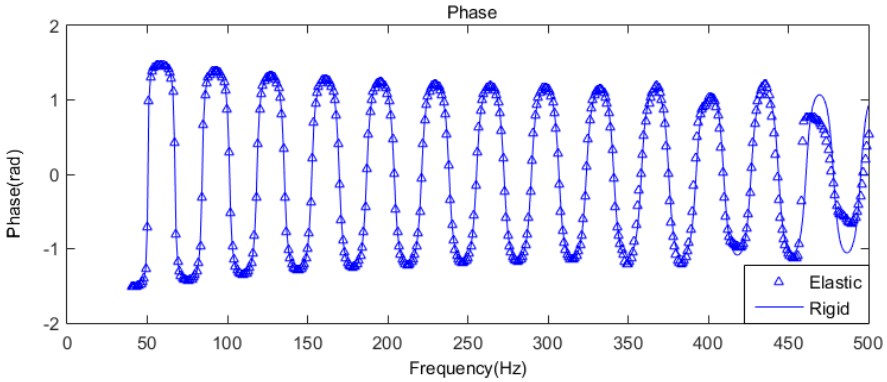

(b)

Figure 3. Comparison with the elastic model: (a) Magnitude, (b) Phase

3.1.2. External problem. For the case of an external problem, a sound radiation test of a 1:5 reduced scale rail above a layer of melamine foam has been chosen for which a numerical result and experimental data are available [15]. This is illustrated in Figure 4. In this case the rail is modelled by boundary elements and the foam is modelled by the poroelastic finite elements. As the properties of the foam are unknown, they had to be determined by either simulation or measurement. This process is described in Section 4.

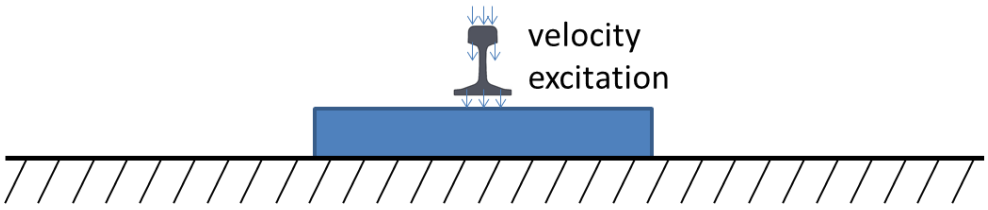

Figure 4. External problem: a 1:5 scale rail above a layer of melamine foam

A unit vertical velocity is given around the rail and the ground is assumed to be rigid. The result is shown in Figure 5 in terms of the radiation ratio of the rail. The dashed black line is obtained from the 2D boundary element method with a semi-analytical model for the porous material impedance, which includes the effect of thickness of the foam. The solid blue line is from the developed model, which agrees well with the black line. The difference between the two models is very small, as the frame of the foam is hardly excited by the acoustic radiation of the rail. The two lines show discrepancies at low and high frequencies against the measured data, but overall the graph shows good agreement with an acceptable deviation.

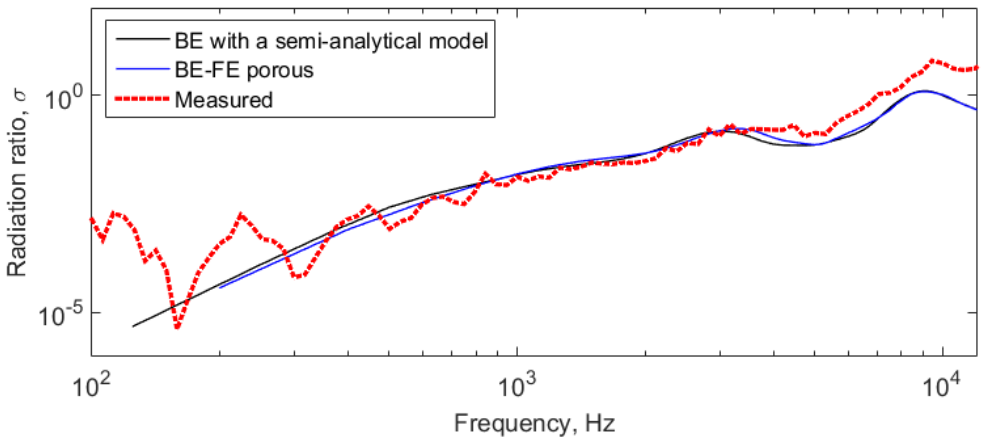

Figure 5. Radiation ratio: a 1:5 scale rail above melamine foam

4. Characterisation of porous materials

As mentioned in the last section, the properties of the material need to be quantified to be put into the model. The properties can be divided into two types. One consists of properties which were introduced in the rigid model ("rigid properties"), and the other is properties from the elastic model ("elastic properties"). A range of methods have been developed either to measure or inversely characterise these properties. In this paper the rigid parameters have been found by inverse characterisation from measured impedance data. These are listed in Table 2. However, for the elastic parameters, a more accurate analysis is necessary as different combinations of elastic parameters can lead to the same result. This is illustrated in Figure 6 and Figure 7, for example. For the foam used previously, absorption coefficient data measured in an impedance tube has been used as a reference. The red lines in the two graphs indicate that two different parameter combinations show nearly the same result. The black line in the first graph shows the result from the rigid model, which cannot predict the effect of frame resonance around 900 Hz.

Table 2. Rigid properties of the melamine foam

Property	α_∞	ϕ	σ (Ns/m^4)	Λ (μm)	Λ' (μm)
Value	1.06	0.97	10000	150	200

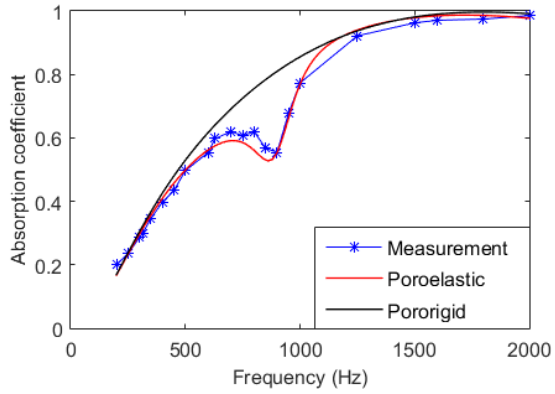

Figure 6. Comparison with the measured absorption coefficient from impedance tube measurement: $E = 300000$ Pa, $\nu = 0.2$

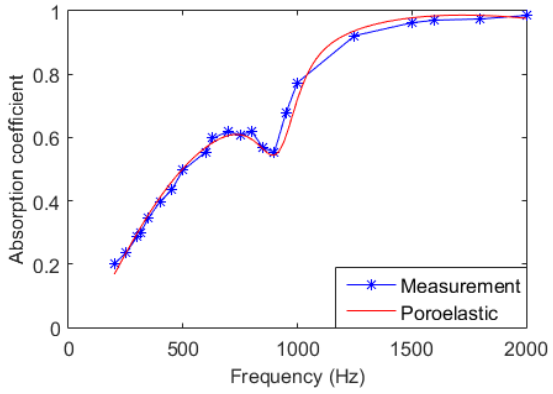

Figure 7. Comparison with the measured absorption coefficient from impedance tube measurement: $E = 94000$ Pa, $\nu = 0.45$

In this paper, a method by Langlois [16] has been used to determine the elastic parameters. It consists of a dynamic stiffness measurement and finite element simulations. From the measurement the dynamic stiffness and its loss factor can be obtained. On the other hand, a polynomial relation between the Young's modulus and the Poisson's ratio can be derived from the simulation. By combining those one could get a Young's modulus as a function of Poisson's ratio. Using a second sample with a different aspect ratio, another function is obtained. By plotting the two curves from the different samples, unique values of Young's modulus and Poisson's ratio can be obtained from their intersection.

4.1. Dynamic stiffness measurement

For the sample foam used in the previous section, the dynamic stiffness has been measured. The measurement setup is depicted in Figure 8. It consists of a disk-shaped sample of porous material placed between two rigid plates. A large mass (31 kg) made of steel is located at the bottom to provide a blocked termination. An accelerometer is placed on the top plate and a force gauge between the lower plate and the mass. The sample is excited by a shaker, fixed on the holder, at angular frequency ω. The ratio between two measured values gives the dynamic stiffness of the sample, as:

$$Z_{\mathrm{m}}(\omega) = \frac{F(\omega)}{u(\omega)} = K_{\mathrm{m}}(\omega)\big(1 + j\eta(\omega)\big) \tag{19}$$

where $F(\omega)$ and $u(\omega)$ are the force transmitted to the mass and the displacement of the sample surface. This can also be expressed by using the dynamic stiffness with real part $K_{\mathrm{m}}(\omega)$ and loss factor $\eta(\omega)$. The measurement can be regarded as quasi-static if the excitation is well below the resonance frequency of the sample. Also, the strains applied to the sample should be less than 5% to ensure linearity in the sample [17]. Both conditions enable the sample to have in vacuo-like behaviour.

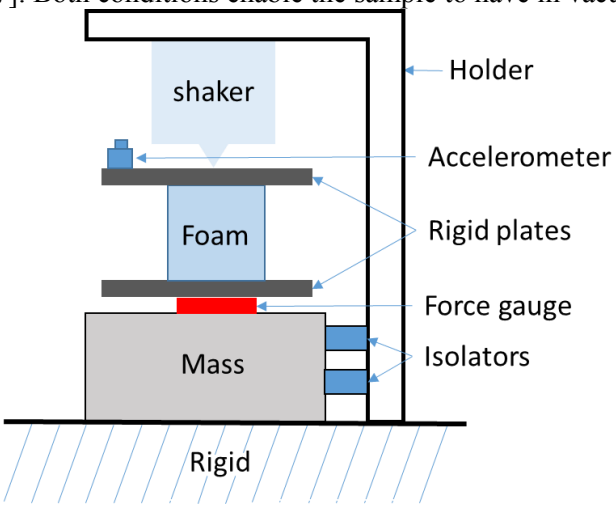

Figure 8. Setup for dynamic stiffness measurement

4.2. Finite element simulation

The finite element analysis of the quasi-static measurement is needed to extract the relationship between the stiffness and the Poisson's ratio. It can be done by varying the Poisson's ratio for a given arbitrary Young's modulus. In the finite element simulation the sample is modelled as a pure solid material. For a narrow sample Young's modulus is related to the stiffness by

$$K_0 = \frac{EA}{L} \tag{20}$$

where L is the length, A the area of the upper surface and K_0 the compression stiffness which is assumed as an arbitrary value. From the simulation, an apparent Young's modulus is obtained from

$$K_{\mathrm{m}}(0) = \frac{E'A}{L} \tag{21}$$

where K_{m} is the computed compression stiffness from the FE analysis which depends on the shape of the sample and on the Poisson's ratio. Dividing Equation (21) by Equation (20) yields the normalised ratio of the static compression stiffness.

$$\frac{E'}{E} = \frac{K_{\mathrm{m}}(0)}{K_0} \tag{22}$$

For a given aspect ratio, this ratio can be plotted as a function of Poisson's ratio. This function can be approximated as a polynomial function of ν, namely:

$$P_{\mathrm{s}}(\nu) = \frac{K_{\mathrm{m}}(0)}{K_0} = 1 + \sum_{i=1}^{N} D_i^{\mathrm{s}} \nu^i \tag{23}$$

From the quasi-static approximation,

$$K_{\mathrm{m}}(\omega) \to K_{\mathrm{m}}(0) \text{ for } \omega \ll \omega_1 \tag{24}$$

where ω_1 is the first resonance frequency of the frame. If two different samples are used, the corresponding Young's moduli can be calculated in both cases as a function of Poisson's ratio and they should be the same since it is an intrinsic property. From Equation (22),

$$E = \frac{E'}{K_{\mathrm{m}}(0)/K_0} = \frac{E'}{P_{\mathrm{s}}(\nu)} \tag{25}$$

From Equations (21), (23) and (25),

$$E = \frac{K_{\mathrm{m,s1}}(\omega)L_{\mathrm{s1}}}{A_{\mathrm{s1}}P_{\mathrm{s1}}(\nu)} \tag{26}$$

$$E = \frac{K_{\mathrm{m,s2}}(\omega)L_{\mathrm{s2}}}{A_{\mathrm{s2}}P_{\mathrm{s2}}(\nu)} \tag{27}$$

Combining Equations (26) and (27) yields

$$\frac{K_{\mathrm{m,s1}}(\omega)L_{\mathrm{s1}}}{A_{\mathrm{s1}}P_{\mathrm{s1}}(\nu)} = \frac{K_{\mathrm{m,s2}}(\omega)L_{\mathrm{s2}}}{A_{\mathrm{s2}}P_{\mathrm{s2}}(\nu)} \tag{28}$$

By applying the quasi-static condition, Equation (28) becomes purely an equation in Poisson's ratio. Solving this polynomial equation gives a unique solution for Poisson's ratio. Once this is done, the Young's modulus can also be determined.

4.3. Elastic parameters of the melamine foam

Two samples of foam of the same diameter but with different thickness have been used as shown in Figure 9. The diameter is 100 mm in each case, and the thicknesses are 52 mm and 18 mm, respectively. The results from the measurement are shown in Figure 10. The values in the graphs are within a certain range so as a first attempt the range has been used to include this uncertainty. It should be noted that the condition of the sample surface is critical to the result, so it should be clean and well attached to the both plates otherwise the upper plate can vibrate on the sample surface. Also, the resonance peaks in the measurement are thought to be due to the test-rig frame.

(a) (b)

Figure 9. Samples: (a) Thick, (b) Thin

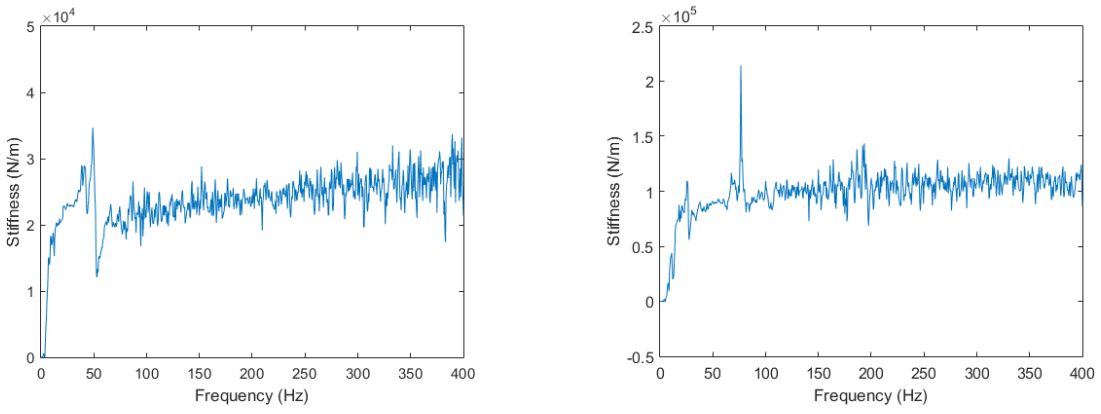

(a) (b)

Figure 10. Measured dynamic stiffness: (a) Thick, (b) Thin

The finite element simulation for each sample has been done by using a commercial software ABAQUS. A Young's modulus curve has been obtained from this and represented by a polynomial. This is illustrated in Figure 11.

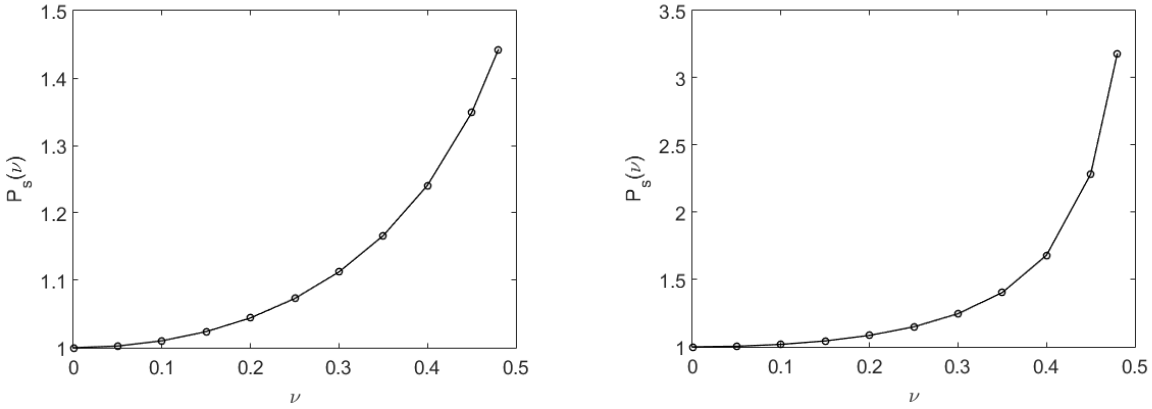

(a) (b)

Figure 11. Simulation results: (a) Thick, (b) Thin

The polynomial relation obtained by regression for each sample is

$$P_{s1}(\nu) = 134.2\nu^6 - 153.2\nu^5 + 70.82\nu^4 - 14.24\nu^3 + 2.348\nu^2 - 0.0447\nu + 1 \quad (29)$$

$$P_{s2}(\nu) = 1784\nu^6 - 1904\nu^5 + 789.8\nu^4 - 148.7\nu^3 + 14.51\nu^2 - 0.3785\nu + 1 \quad (30)$$

Combining the results with Equations (26) and (27), taking K_m as the input, the Young's modulus curves can be obtained. The result is also given as a range, as shown in Figure 12. From the two ranges, a set of possible solutions can be obtained. To see the variance of the solution, a comparison has been made with the measured absorption coefficient in Figure 6. The values in Table 3 have been used to provide a set of possible results, as shown in Figure 13.

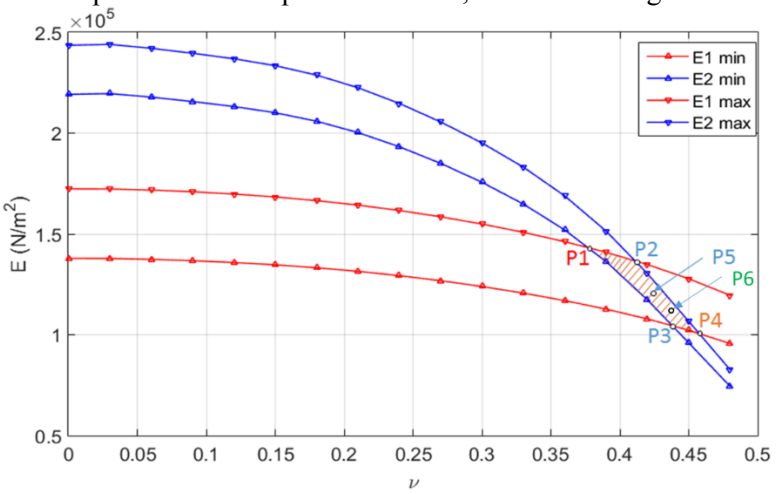

Figure 12. Young's modulus curves: red lines-thick sample, blue lines-thin sample. The solution exists in the shaded region.

Table 3. (E, ν) for the selected points

	E(kPa)	ν
P_1	143.5	0.377
P_2	137.0	0.412
P_3	104.5	0.438
P_4	101.0	0.458
P_5	122.0	0.425
P_6	110.0	0.441

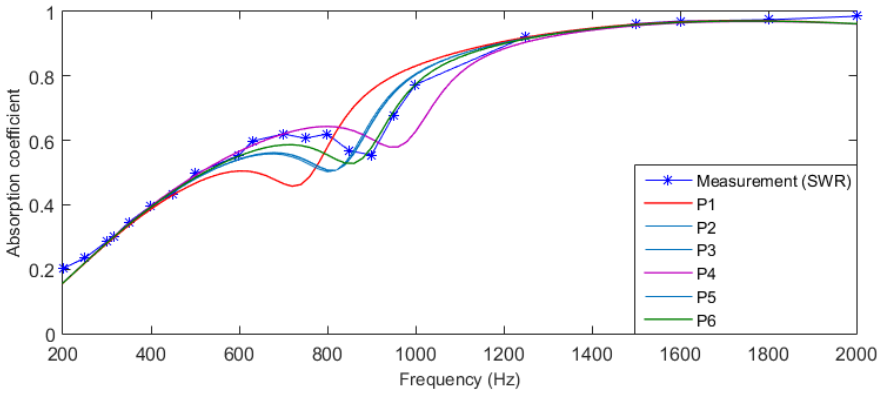

Figure 13. Comparison of absorption coefficient with the measured data

The two points at both ends, P_1 and P_4, show the limits of the result. The other points which are located in the middle, show nearly an identical result, with the dip at 820 Hz. Overall, it can be said that the median values give acceptable results. From the result the elastic properties of the foam are obtained, as shown in Table 4. Note that the loss factor η has been obtained from the imaginary part of the measured stiffness.

Table 4. Elastic properties of the melamine foam

Property	E (kPa)	η	ν
Value	122 ± 15	≤ 0.1	0.425 ± 0.013

5. Conclusions

A 2D numerical modelling of porous material including its elasticity has been implemented and coupled to the acoustic boundary element method. It has been validated for internal and external problems. It has been shown that the elasticity has an effect on the absorption at the frame resonance frequencies. From the external case it has been noted that simple models could work for cases where the rail vibration hardly affects the absorptive treatment. A simple way consisting of a dynamic stiffness measurement and a finite element simulation has been used to determine the properties of porous materials. From the measurement it has been noted that the condition of the sample surface is important in order to attach the sample to the holding structure. The measured stiffness has been determined within a range. The use of median value gave an acceptable agreement with the measured data.

Acknowledgement

This research was supported by a grant (15RTRP-B072484-03) from Railroad Technology Research Program funded by Ministry of Land, Infrastructure and Transport of Korean government.

References

[1] Thompson D 2008 *Railway noise and vibration: mechanisms, modelling and means of control* (Amsterdam: Elsevier)
[2] Jean P 1998 A variational approach for the study of outdoor sound propagation and application to railway noise *J. Sound Vib.* **212** 275-294
[3] Morgan P, Hothersall D and Chandler-Wilde S 1998 Influence of shape and absorbing surface—a numerical study of railway noise barriers *J. Sound Vib.* **217** 405-417
[4] Biot M A 1956 Theory of Propagation of Elastic Waves in a Fluid-Saturated Porous Solid. I. Low-Frequency Range *J. Acous. Soc. Am.* **28** 168-178
[5] Biot M A 1956 Theory of Propagation of Elastic Waves in a Fluid-Saturated Porous Solid. II. Higher Frequency Range *J. Acous. Soc. Am.* **28** 179-191

[6] Atalla N, Panneton R and Debergue P 1998 A mixed displacement-pressure formulation for poroelastic materials *J. Acous. Soc. Am.* **104** 1444-1452
[7] Allard J F and Atalla N 2009 *Propagation of sound in porous media : modelling sound absorbing materials* (Hoboken, N.J.: Wiley)
[8] Johnson D L, Koplik J and Dashen R 1987 Theory of dynamic permeability and tortuosity in fluid-saturated porous media *J. Fluid Mech.* **176** 379-402
[9] Champoux Y and Allard J F 1991 Dynamic tortuosity and bulk modulus in air-saturated porous media *J. Appl. Phys.* **70** 1975-1979
[10] Dauchez N, Sahraoui S and Atalla N 2001 Convergence of poroelastic finite elements based on Biot displacement formulation *J. Acous. Soc. Am.* **109** 33-40
[11] Hörlin N-E 2004 Hierarchical finite element modelling of Biot's equations for vibro-acoustic modelling of layered poroelastic media
[12] Rigobert S, Atalla N and Sgard F 2003 Investigation of the convergence of the mixed displacement-pressure formulation for three-dimensional poroelastic materials using hierarchical elements *J. Acous. Soc. Am.* **114** 2607-2617
[13] Wu T 2000 *Boundary element acoustics: Fundamentals and computer codes* (Southampton: Wit Pr/Computational Mechanics)
[14] Debergue P, Panneton R and Atalla N 1999 Boundary conditions for the weak formulation of the mixed (u, p) poroelasticity problem *J. Acous. Soc. Am.* **106** 2383-2390
[15] Zhang X, Squicciarini G and Thompson D J 2016 Sound radiation of a railway rail in close proximity to the ground *J. Sound Vib.* **362** 111-124
[16] Langlois C, Panneton R and Atalla N 2001 Polynomial relations for quasi-static mechanical characterization of isotropic poroelastic materials *J. Acous. Soc. Am.* **110** 3032-3040
[17] Hilyard N and Cunningham A 2012 *Low density cellular plastics: physical basis of behaviour* (London: Springer Science & Business Media)